Lifetime of Wannier-Stark states in semiconductor superlattices under strong Zener tunneling to above-barrier bands

B. Rosam and K. Leo*
Institut für Angewandte Photophysik, Technische Universität Dresden, 01062 Dresden, Germany

M. Glück, F. Keck, H. J. Korsch,† and F. Zimmer
Fachbereich Physik, Universität Kaiserslautern, 67653 Kaiserslautern, Germany

K. Köhler
Fraunhofer-Institut für Angewandte Festkörperphysik, 79108 Freiburg, Germany
(Received 5 November 2002; revised manuscript received 14 April 2003; published 2 September 2003)

For high electric fields, the lifetime of Wannier-Stark ladder states in a periodic potential is reduced by the fundamental process of Zener tunneling. We report on the analysis of the coherence lifetime of such states in semiconductor superlattices by interband spectroscopy. The reduction of lifetime by strong coupling between bands can only in the first approximation be described by the well-known Zener theory. A recently developed theoretical model is applied to calculate directly the tunneling probability of Wannier-Stark states as a function of the electric field. The theoretical results compare well with experiment, reproducing the complex interplay of both nonresonant and resonant Zener tunneling to higher bands. By comparing experiment and theory for a superlattice with a symmetric and one with a nonsymmetric potential, we can draw conclusions on a very general basis about the sensitive dependence of Zener tunneling on the specific dispersion relation of the carriers.

DOI: 10.1103/PhysRevB.68.125301 PACS number(s): 72.20.Ht, 73.21.Cd, 78.47.+p, 78.66.−w

I. INTRODUCTION

The energy spectrum of carriers in a periodic potential under a static electric field has been an issue of intense research due to its fundamental importance for optical and transport properties of solids. In semiconductor superlattices[1] (SSLs), a periodic modulation of conduction- and valence-band edges leads to an artificial periodic potential (superimposed on the atomic potential) for the carriers, splitting their energy spectrum into minibands (MBs). The design of a SSL geometry allows one to tailor the band structure of carriers and, consequently, SSLs became a model system to investigate the quantum states of a periodic potential and their dynamics. With the first observation of Wannier-Stark states in a SSL,[2] a long-standing theoretical debate about the their physical existence ended in 1988. Already in 1960, Wannier[3] had found that the energy spectrum of carriers, subject to a periodic potential and an electric field F, consists of equally spaced eigenvalues, the Wannier-Stark ladder (WSL), with an energy splitting scaling linearly with the electric field. However, he had already pointed out that the associated states are metastable due to tunneling. This was emphasized by Avron *et al.*,[4] proving that the energy spectrum in general is continuous. Nevertheless, at low fields where the tunneling probability is low compared to other characteristic scattering rates of the system, the problem can be well described by common approximations, e.g., by the tight-binding approach,[5] which lead to stationary states.

Recently, key results of experiment and theory have shown that tunneling can play a decisive role. Based on the interaction of a finite number of bands, the signature of resonant tunneling between discrete Wannier-Stark states has been shown in experiment[6–10] and was described by theory.[11–16]

Recently, the signature of electrical breakdown in SSLs was observed directly in the optical spectrum.[17] The observations were compared to the theory by Glutsch and Bechstedt,[18] who showed numerically that at high fields the coupling of, in principle, an infinite number of bands causes the concept of localized WSL states to fail totally. Instead, a tunneling-induced spatial delocalization of the states is observed.[17] This is associated with a reduction of the coherence lifetime due to an increased tunneling probability of the state. It was found that the field dependence of the lifetime of WSL states shows a complex behavior. Apart from a continuous decrease, oscillations are observed which can be attributed to resonant tunneling.

In his well-known paper, Zener[19] calculated the tunneling rate γ of an electron from one band through a band gap into a second band:

$$\gamma(F) = \frac{ed|F|}{2\pi\hbar} \exp\left(\frac{-m_e d(\Delta E)^2}{4\hbar^2 e|F|} \right), \tag{1}$$

with d here being the SSL period, m_e the effective electron mass, and ΔE the band gap. This equation, referred to as the Zener equation, predicts a continuous increase of tunneling as a function of field. This effect is known as *nonresonant* Zener tunneling. It cannot describe the effects of *resonant* Zener tunneling between WSL states.

So far, the relationship between nonresonant and resonant Zener tunneling for a certain band structure remained unclear. To our knowledge, Bharucha *et al.*[20] showed for the first time in an alternative periodic system, atoms in an accelerating optical lattice, that the tunneling probability shows

both resonant and nonresonant features, but the effect was only measured for a very small field interval.

Here, we present a comprehensive experimental and theoretical study which investigates in a solid-state system the interplay of nonresonant and resonant Zener tunneling. A theory developed by Glück *et al.*,[21] calculates directly the tunneling probability of the states. Second, experimental results of a second SSL structure are presented which show a distinctively different dependence of the states lifetime on the electric field. Using our results we can draw basic conclusions on how the complex behavior of Zener tunneling is defined by different band structures and will help to understand the limitations of the classical Zener equation.

II. EXPERIMENT

For our study of the Zener effect, strongly coupled SSLs with low barriers were used. The structures were designed to have only one electron MB energetically below the band edge of the barrier at zero field. Therefore, the Zener effect observed is caused by the Zener tunneling from the lowest MB into above-barrier MBs. In these shallow SSLs, tunneling plays a decisive role at low fields. Therefore, these structures have been proven to be very suitable to explore tunneling over a wide field range. In this paper, we present results of two SSL geometries for sample *A*, a $GaAs/Al_{0.08}Ga_{0.92}As$ SSL (well width $a=76$ Å; barrier width $b=39$ Å; barrier height for electrons $H_e=62$ meV; and barrier height for holes $H_h=46$ meV), and sample *B*, a $GaAs/Al_{0.11}Ga_{0.89}As$ SSL ($a=50$ Å, $b=54$ Å, $H_e=83$ meV, and $H_h=64$ meV) structure.

Both samples consist of 35 undoped SSL periods and different buffer layers to ensure a linear drop of the electric field across the SSL. A semitransparent Schottky contact (Au/Cr) inhibits electron injection. For the transmission measurements, the substrate was removed by wet etching.

The SSL geometry of the structures was designed (with the help of a transfer-matrix-model) to investigate strong coupling to above-barrier states. Both samples were intended to have the same bandwidth of the first electron MB of about 30 meV and the same energetic distance of the center of the first electron MB to the upper edge of the barrier of about 30 meV. The main difference between the samples is that sample *B* has a symmetric geometry, i.e., well and barrier are almost equal in width. This resembles a cosine potential and one expects small gaps between the upper MBs.[38]

Since the influence of tunneling on the energy spectrum (and the associated wave functions) and the lifetime of the states of a SSL becomes obvious in the optical spectrum of the system, we measured the linear interband absorption of the SSL as a function of the field. The sample was illuminated by a halogen lamp and held at a temperature of 10 K. Due to their high effective mass, holes are already localized at low fields and the field-dependent change of the absorption is defined predominantly by the electron states. Therefore, absorption measurements can be used to study exclusively that how tunneling coupling affects the electron WSL states. The homogeneous linewidth Γ of an interband absorption line is linked to the total polarization scattering rate of the transition, which is the sum of the scattering rates for an electron and a hole.

III. THEORETICAL DESCRIPTION

To theoretically describe absorption $D(\omega)$ we use a model developed in Ref. 22. The analytic approach behind the numerics is a specific scattering theory developed in Refs. 21,23–25. The model results in the calculation of metastable WSL states which are the complex-energy poles $\mathcal{E}=E-i\Gamma/2$ of the rigorously constructed scattering matrix. Lifetime τ of the states defined by their tunneling probability follows directly from $\tau=1/\gamma=\hbar/\Gamma$, which corresponds to a line broadening Γ in absorption. Since the optical spectrum is measured in the experiment, an analytic expression was found to describe the absorption spectrum in terms of resonance WSL states.

The absorption of the SSL is dominated by the creation of electron-hole pairs (excitons) and the subsequent decay of the excitons. This can happen in two ways: a recombination of an electron and a hole via Coulomb interaction or by a decay of the electron or hole state due to the applied field. In the high-field regime, the Coulomb interaction can be neglected and the latter process dominates the decay of the exciton state. The exciton state can then be written as

$$|\Psi_{\alpha,\beta,L}\rangle=|\Psi^{e}_{\beta,L}\rangle|\Psi^{h}_{\alpha,0}\rangle, \tag{2}$$

where $|\Psi^{e}_{\beta,L}\rangle$ denotes the electron state at site L and β labels the Bloch band. The same notation holds for the hole state $|\Psi^{h}_{\alpha,0}\rangle$ which is localized at an arbitrary SSL site. The complex energy of the exciton state is given by $\mathcal{E}_L=E^{e}_{\beta}-E^{h}_{\alpha}+E_g+edFL-i(\Gamma^{h}_{\alpha}+\Gamma^{e}_{\beta})/2$, where E_g is the energy gap between the valence and the conduction band and d is the SSL period. Using these notations, it can be shown[22] that the absorption is given by

$$D(\omega)\sim\sum_{\alpha,\beta}\sum_{L}\ \mathrm{Im}\times\left[\frac{I^{2}_{\alpha,\beta}(L)}{(E^{e}_{\beta}-E^{h}_{\alpha}+edFL+E_g-\hbar\omega)-i(\Gamma^{e}_{\beta}+\Gamma^{h}_{\alpha})/2}\right]. \tag{3}$$

Numerator $I^{2}_{\alpha,\beta}(L)$ can be interpreted as the transition matrix element between hole state α and electron state β which are L lattice periods apart. It is given by

$$I^{2}_{\alpha,\beta}(L)=\langle\Psi^{h}_{\alpha,0}|\Psi^{e}_{\beta,L}\rangle\langle\Psi^{e}_{\beta,L}|\Psi^{h}_{\alpha,0}\rangle. \tag{4}$$

Note that $|\Psi^{h}_{\alpha}\rangle$ and $|\Psi^{e}_{\beta}\rangle$ are resonance states and therefore are the non-Hermitian eigenstates of the system. Right and left eigenstates must be distinguished. Generally, they do not coincide (cf. Ref. 26 for details). $I^{2}_{\alpha,\beta}(L)$ depend strongly on the site index L and define the shape and intensity of absorption $D(\omega)$. At $F=0$, Eq. (3) consists of a set of sharp peaks due to the neglect of other broadening effects. In the experiment, for $F=0$ kV/cm, a dominating inhomogeneous broadening was found by comparing the total linewidth in linear

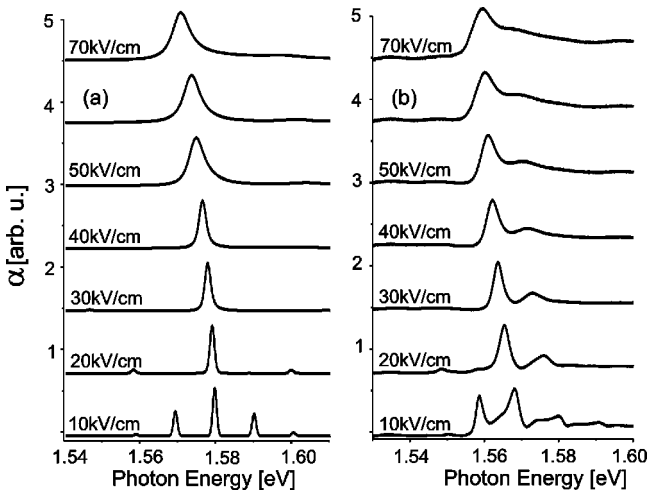

FIG. 1. Normalized absorption spectra of sample B for $F = 10,20,\ldots,70$ kV/cm. (a) Theory. (b) Experiment.

absorption with the homogeneous linewidth determined by degenerate four-wave-mixing experiments (not shown here), e.g., for sample B the inhomogeneous broadening is about 1 meV and the total linewidth is 1.25 meV. This broadening, homogeneous and inhomogeneous, is taken into account field independently by convoluting $D(\omega)$ with a Gaussian to ensure that the width of the main peak at $F=0$ agrees with the experimental data. To compute the absorption dependent on the system parameters, we have to define the shape of the lattice potential. Instead of the usual squared box potential, we have to use an analytic potential since the latter shows a fractal-like dependence of the decay rates of the eigenstates on the field strength.[22] Therefore, we use an analytic potential of the following form:

$$V(x)=\frac{V}{2}\{\tanh[\sigma(x+b/2)]-\tanh[\sigma(x-b/2)]\}, \quad (5)$$

which is a smoothed square box potential of width b and where σ defines the smoothness of the potential. The shape of the potential is assumed to be the same for electrons and holes and the effective masses are assumed to be constant.

As an example, Fig. 1 shows calculated absorption spectra of sample *B* and compares them with the experiment. The theory calculates the energy spectrum relative to the band-gap energy which here was added with $E_g(\mathrm{GaAs}) = 1.52$ eV for comparison with experiment. In the plotted energy interval, the transitions from the first heavy-hole (hh) MB to the first electron MB, i.e., the $\alpha=1$ to $\beta=1$ transitions, are shown. On the left-hand side, the theoretical spectra are given. For $F=10$ kV/cm, the WSL transitions from the localized hole state to the delocalized electron states are seen clearly, whereas the central peak can be attributed to the direct transition from $\alpha=1$ to $\beta=1$ within one SSL layer ($L=0$), i.e., the (1,1)-hh_0 transition. The neighboring peaks are contributions of indirect ($L\neq 0$) WSL transitions. For $F = 20$ kV/cm, the WS localization[2] implies that only the $(1,1)-\mathrm{hh}_0$ transition remains (only very weak $L=\pm 1$ transitions are still seen). In a one-band picture, which neglects tunneling, a single $L=0$ peak, not changing with increasing field, would be the high-field limit. Instead, the model predicts a peak which for higher field broadens strongly and is red shifted. This is due to the increasing tunneling probability which is calculated directly by the theory. The resulting linewidth of the transition mirrors the reduced states lifetime.

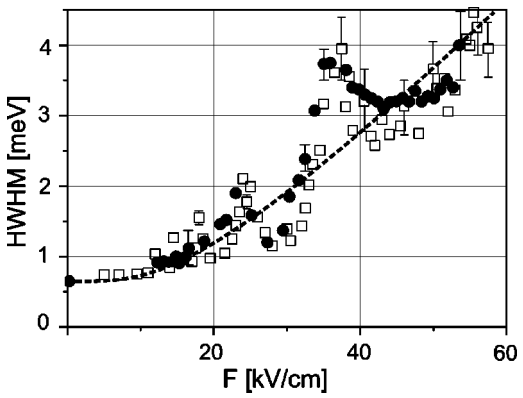

FIG. 2. Sample *A*: Linewidth Γ of the (1,1)-hh_0 WSL transition as a function of electric field F. Experiment (solid circles), theory (hollow squares), and fit with Eq. (1) (dashed line).

On the right-hand side of Fig. 1, the experimental spectra are plotted. Please keep in mind that theory uses a one-dimensional model and does not include Coulomb interactions and light holes. Nevertheless, especially for high field $F>30$ kV/cm, where tunneling plays a dominating role, theory compares well with experiment. The predicted line broadening of the (1,1)-hh_0 transition caused by tunneling is observed clearly. For $F>20$ kV/cm, the weak absorption peak, which is seen at the high-energy side of the main peak, can be attributed to the $(1,1)L=0$ transition of the light hole. For 10 kV/cm, in the WSL regime, the experimental spectrum shows the well-known features of Coulomb interaction.[27–30] The Coulomb interaction and the uncertainties concerning the effective masses of the carriers and the exact SSL potential are the reasons for the deviation of the absolute energy scale between experiment and theory.

IV. RESULTS

To monitor the field dependence of the WSL state's lifetime, we measured field-dependent absorption spectra and analyzed the linewidth of the direct interband WSL transition (the transition within one quantum well layer of the SSL), i.e., the (1,1)-hh_0 WSL transition.

A. Sample *A*

First, let us look at sample *A*. Figure 2 displays the linewidth [half-width at half maximum (HWHM)] of the (1,1)-hh_0 WSL transition measured as a function of the field (these data were presented earlier[31]). The absorption line of this particular transition was fitted by a Gaussian peak. For medium fields $F=10$–20 kV/cm, in the WSL regime, where the electron has a certain probability density in the neighboring wells, the linewidth stays almost constant. In this field region, excitonic coupling leads to the Fano broadening of the line,[27] causing an asymmetric line shape. Therefore, in

this field range the line can only be fitted approximately by the present method. However, we here concentrate on higher fields at which the Wannier-Stark localization of the electron wave function suppresses the Fano coupling and broadening, due to Zener tunneling starts to dominate. For fields $F > 30$ kV/cm, the linewidth increases drastically. The coupling to states of higher bands is no longer negligible.

From the original Zener theory[19] one would expect a continuous increase of the linewidth. To underline this, we also plot here the fit by the Zener equation, Eq. (1), as in our previous paper (cf. Fig. 2 of Ref. 31). The fit can only describe the overall behavior. In contrast, the graph clearly shows strong oscillations which can be attributed to resonant coupling of WSL states of the first with states of the second electron MB. These resonances are seen as anticrossings of WSL states in the absorption spectra and will be discussed in more detail in Sec. V.

The graph also presents the results of the theory. The interplay of the continuous increase of the linewidth due to nonresonant Zener tunneling and the peaks due to resonant Zener tunneling are reproduced effectively. To be more specific, the numerical data were obtained by computing the energy levels and states in the valence and the conduction band using the method described in Refs. 33 and 32 and fitting a Gaussian to the dominant peak of $D(\omega)$. Exemplary error bars, both for experiment and theory, are plotted to account for uncertainties of the fitting. For theory, the fitting is approximate for strong fields and in the vicinity of resonances because the line shape becomes asymmetric. In experiment, for a strong field only the low-energy side of the absorption can be fitted, since on the high-energy side in-plane absorption and the light-hole transition are superimposed. Additionally, the strong weakening, i.e., the decreasing oscillator strength, of the transition causes higher uncertainties.

In our theoretical description, we use scaled variables where the dimensions are defined by setting the lattice period equal to 2π, the masses to one, and the potential heights equal to two. This leads to a dimensionless scaled Planck constant given by $\hbar_s = 2\pi\hbar/(d\sqrt{Vm})$ (cf. Ref. 32 for details). Using the parameters for sample *A*, we get a scaled Planck constant $\hbar_s^e = 3.3$ for the electrons and $\hbar_s^h = 1.5$ for the holes. For these parameters, the decay rates of the exciton states are given mainly by the decay of the electron contribution. To take into account experimental uncertainties, e.g., the heights of the potential barriers or the effective masses, we used a Metropolis algorithm which allows the slight variations of the parameters $\hbar_s^e$, $\hbar_s^h$, and σ to improve the agreement between experiment and theory. This procedure led to the optimized values $\hbar_s^e = 3.1$, $\hbar_s^h = 1.5$, and $\sigma = 2.5$.

As mentioned earlier, theory introduces a certain smoothing of the potential to describe the experimental results. There is no doubt that a rectangular potential cannot be realized in nature since the Al atoms are distributed randomly in the barrier. The effects of alloy fluctuation and interface roughness have been subjects of several papers, e.g., see Refs. 34–36. For future investigations, it would be desirable to measure directly the abruptness of the potential barriers to support our results. A smoothing of $\sigma = 2.5$ corresponds to a deviation from rectangular potential by 3 ML (monolayers), i.e., the distance from the point where the potential reaches 50% of the barrier height to the points where the potential reaches 10% or 90% of the barrier height.

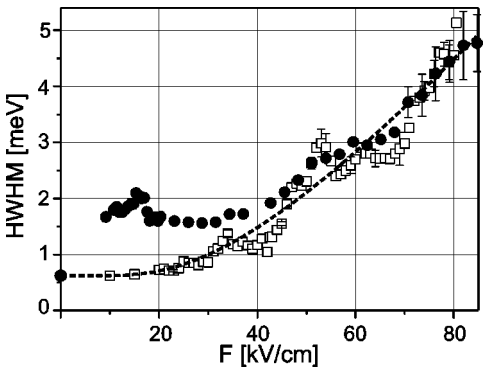

FIG. 3. Sample *B*: Linewidth Γ of the (1,1)-hh$_0$ WSL transition as a function of electric field *F*. Experiment (solid circles), theory (hollow squares), and fit with Eq. (1) (dashed line).

B. Sample *B*

For comparison, Fig. 3 displays the field dependence of the linewidth (HWHM) of the (1,1)-hh$_0$ transition for sample *B*. Contrary to sample *A*, sample *B* seems to follow the Zener equation. Only very small oscillations due to resonant tunneling can be found.

Theory can also reproduce this behavior in detail. By following the same procedure as for modeling sample *A*, we again get optimized values for the scaled Planck constants to fit the experiment. For sample *B*, they read $\hbar_s^e = 2.9$, $\hbar_s^h = 1.2$, and $\sigma = 1.3$. Note that the potential obtained for the best agreement with experiment has a larger smoothing than for sample *A*, which here corresponds to a deviation from rectangular potential by 5 ML (see discussion in Sec. IV A). Using these values, we arrive at the linewidths which are shown in Fig. 3 in comparison to the experimental data.

The linewidth follows Zener's theory, with only a marginal structure superimposed. Therefore, we use Eq. (1) to fit the experimental data of sample *B* in Fig. 3. To account for the linewidth at $F = 0$ a constant was added. From the fit, the band gap E_{12} between the first and the second electron MB can be extracted. We get $E_{12} = 51$ meV which is in reasonable agreement with the band gap obtained from the dispersion relation, which will be presented in the following section. In principle, it is surprising that the Zener equation can fit the behavior well since this semiclassical theory should fail for high field.

V. DISCUSSION

To discuss the physics behind the different behavior of samples *A* and *B*, let us have a look at the dispersion relations of both potential geometries in the field-free case which are displayed in Fig. 4. These were calculated with the potentials used for modeling the linewidth. The main difference—besides the widths of the individual bands—is

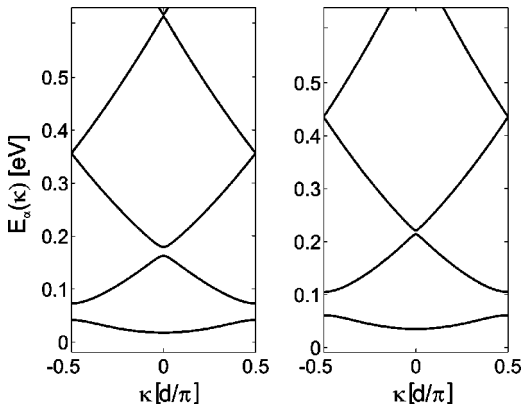

FIG. 4. Dispersion relation of the SSL minibands of the electron for sample *A* (left) and sample *B* (right).

given by the size of the gaps. Sample *B* has an approximately symmetric potential ($a \approx b$), leading to a dominant first coefficient in the potential's Fourier expansion. Therefore, higher Fourier coefficients are small, leading to small higher gaps.[38] Here, we compare the first two gaps E_{12} and E_{23} which influence mainly the Zener effect, since the size of higher gaps becomes very small. These are equal to $E_{12} = 31/44$ meV and $E_{23} = 17/7$ meV for sample A/B. In comparison to sample *A*, the gap between the first and the second MB is larger for sample *B* and the gap to the third MB is much smaller. These are the reasons that on one hand the overall coupling (between the lowest electron WSL state and higher states) is weaker for sample *B* mainly due to the large first gap. On the other hand, the small second band gap for sample *B* leads to strong coupling between the above-barrier bands which inhibits resonant tunneling.

This is also illustrated in Fig. 5 where the calculated field-dependent tunneling rates, the imaginary part of the energy,

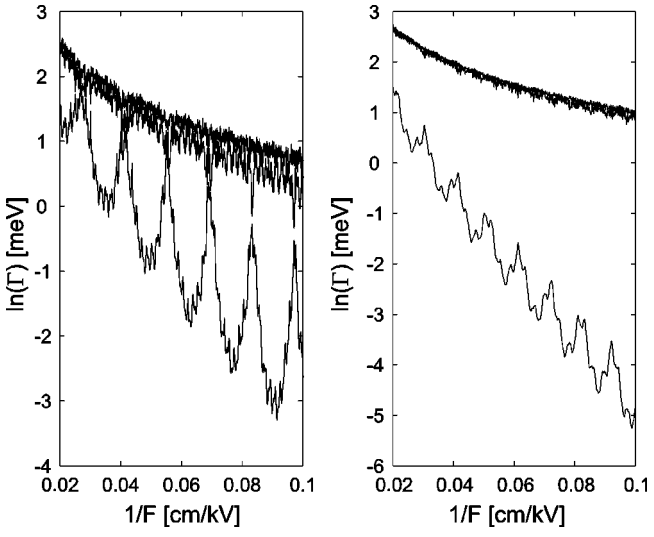

FIG. 5. Dependence of the imaginary parts of the three most stable electron MB energy levels on the inverse field strength for sample *A* (left) and sample *B* (right). For sample *B*, the excited states can no longer be distinguished and act as a quasicontinuum for the ground state.

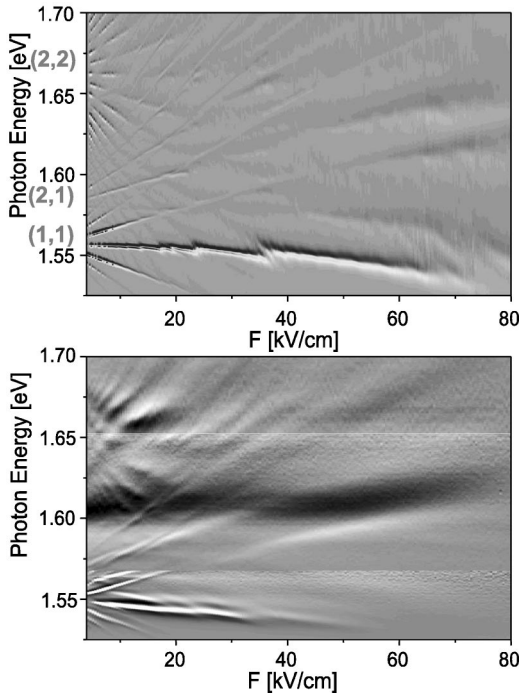

FIG. 6. Wannier-Stark fan for sample *A*: The figure shows the absorption dependent on the field strength *F* and the photon energy $h\nu$. Theory (top). The numbers in brackets (α,β) label the fans of WSL transitions between the hole MB α and the electron MB β. Theory considers a GaAs-band-gap energy of 1.52 eV. Experiment (bottom).

of the three most stable conduction band-energy levels are compared. For sample *B*, the first state is well separated from the others, whereas the two higher states are nearly indistinguishable. In comparison, for sample *A*, the plot shows clearly tunneling resonances as peaks of the first state's decay rate. Contrary to sample *B*, the two above-barrier states can be resolved.

A look at the optical spectra provides a possibility to have a more comprehensive point of view on how the single WSL transitions evolve and how they are affected by tunneling. Here, the so-called Wannier-Stark fan diagrams for both structures are compared. The gray scale map plots absorption spectra along the energy axis as a function of the field. For the experimental plot, three separate measurements in three energy intervals were merged; whereas, the spectra, separately for each interval, had to be corrected for the spectral response of the experimental apparatus and differentiated along the energy axis to make weak transitions visible. Therefore, one has to keep in mind that the intensities of the transitions in the different energy intervals cannot be directly compared. For comparison, theory also plots the derivative $\partial D/\partial\omega$.

Figure 6 presents experiment and theory for sample *A*. The low-energy part of the experimental plot was already presented in Ref. 17, but the extended energy scale, however, will provide a better understanding. Let us first look at the theory showing the main features more clearly, since it does not include excitons, light-hole transitions, and is devoid of

noise. Two prominent fanlike structures can be identified. The lower, more prominent fan corresponds to the transition between the most stable states, the first electron and the first hole MB, $\alpha=1\rightarrow\beta=1$. The central branch of this fan can be associated directly with the (1,1)-hh_0 transition. The neighboring branches correspond to transitions with $L=\pm1$, $L=\pm2$, etc. Following the central branch, gaps are observed where resonant tunneling occurs, marking anticrossings. These can be explained as resonant interactions with states of the second electron MB, which originate from a Wannier-Stark fan centered at an energy of about 1.66 eV. This fan corresponds to transitions of the second hole MB to the second electron MB, $\alpha=2\rightarrow\beta=2$. Energetically, in between these two fans we see the remnants of the transition $\alpha=2\rightarrow\beta=1$ which is weakly allowed.

These structures can also be found in the experimental graph. Besides, Coulomb interaction leads to known features of an excitonic WSL,[28–30] which will not be discussed here. Additionally, light-hole transitions are observed. For light holes the same transitions as for heavy holes are expected, but slightly blue shifted and weaker in strength. The most clearly seen light-hole feature is the doublet of the (1,1) $-(L=0)$ transition. The WSL states of the (1,1) transitions fan out until, due to the Wannier-Stark localization,[2] the off-diagonal WSL transitions vanish. As discussed in Sec. III, contrary to one-band pictures, it is clearly seen that the transitions further change for increasing field strength. Following the (1,1)-hh_0 transition, the effect of nonresonant Zener tunneling increases, which is observed as red shift and consecutive weakening of the transition until it vanishes completely for higher fields. As described above, the (1,1)-hh_0 transition also shows tunneling resonances which are seen as oscillations superimposed on the linewidth of sample *A*, in Fig. 2. These are points of resonant coupling to states of the second electron MB which is above the barrier. The experiment also shows a WSL fan originating from the second electron MB as it was predicted by theory. To our knowledge, this is the first time that WS localization of unconfined states is observed experimentally. In other words, this verifies that the second band gap E_{23} suppresses the tunneling to the third MB, at least for low fields, strong enough to lead to a spatial localization.

For sample *B*, the lack of interaction of the first electron MB states with higher bands and the strong interaction between the above-barrier bands is mirrored clearly in the Wannier-Stark fan shown in Fig. 7. First, the hh_0 branch of the $\alpha=1\rightarrow\beta=1$ fan does not exhibit the broken feather structure of its counterpart in sample *A*. In fact, the lack of anticrossings in the spectrum in case of coupling to weakly bound states was discussed by Wagner *et al.*[37] and is observed here. Second, in comparison to Fig. 6, it is seen that the weaker fan corresponding to the transition $\alpha=2\rightarrow\beta=2$ is almost absent. Remnants of the fan $\alpha=2\rightarrow\beta=1$, which do not affect the main structure, are still visible. Both, experiment and theory, demonstrate that the small second band gap E_{23} for sample *B* inhibits the spatial localization of the above-barrier states leading to the lack of resonant Zener tunneling.

Let us briefly discuss in rather general terms why the

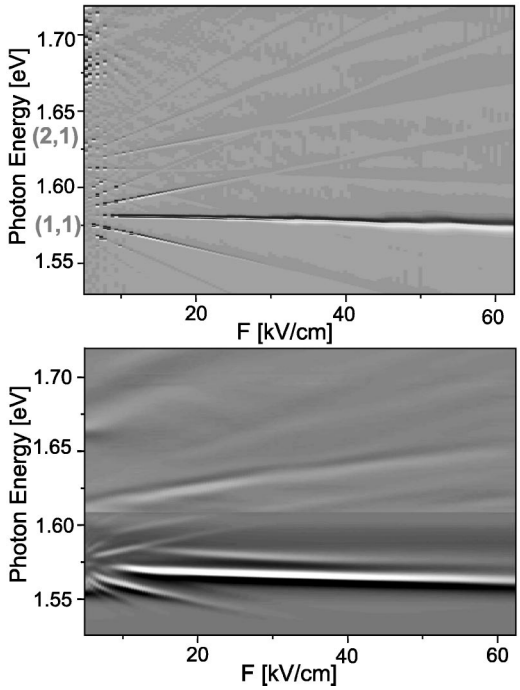

FIG. 7. Wannier-Stark fan for sample *B*: The figure shows the absorption dependent on the field strength F and the photon energy $h\nu$. Theory (top). The numbers in brackets (α,β) label the fans of WSL transitions between the hole MB α and the electron MB β. Theory considers a GaAs-band-gap energy of 1.52 eV. Experiment (bottom).

Zener equation does not describe the admixture of resonant tunneling as observed. Zener[19] only treats the probability of quantum-mechanical tunneling into the next band for carriers at the edge Bloch-state of the Brillouin zone. The tunneling rate follows from the knowledge that the carriers reach the Brillouin-zone edge once per Bloch-oscillation cycle. In his theory, the carriers tunnel virtually into a continuum of states because Wannier-Stark localization is not considered. Additionally, only one Bloch-oscillation period is considered, neglecting any correlations between successive Bloch-oscillation cycles. These assumptions are justified in case the states of the upper band themselves have a very small lifetime due to strong tunneling to higher bands. In other words, this holds if the second band in which the carriers tunnel is empty and the states are weakly bound. In time domain, one can argue that in case of a considerably large second band gap, the intraband coherence time of the carriers in the second band increases. If the coherence time reaches the range of a few Bloch-oscillation cycles, the assumptions of Zener are not valid anymore and in return the effect of resonant tunneling is observed.

VI. CONCLUSIONS

In this paper, we have analyzed the linewidth of WSL transitions in absorption which mirrors the coherence lifetime of the contributing states. It was shown that already for a moderate-field strength, Zener tunneling of the electron WSL state is the dominant line-broadening mechanism.

Therefore, the linewidth was taken as a measure for the tunneling probability of the electron WSL state which could be reasonably well modeled by theory. An interplay of nonresonant and resonant Zener tunneling was observed by investigating two different superlattice structures: a nonsymmetric structure which strongly deviates from the Zener theory by large modulations due to resonant tunneling and a nearly symmetric superlattice which follows Zener's prediction. We have shown that the different tunneling behavior is determined by the dispersion relation of the structures. Here, the main influence comes from the different band gaps of the system. In the first case, sample *A*, a larger second energy gap which separates the second and the third band hampers their coupling by tunneling, which leads to spatial localization of the unconfined states of the second MB (which is energetically above the barrier) and the signature of resonant Zener tunneling. In the second example, sample *B*, the above-barrier bands couple strongly and act as a quasicontinuum for the states of the first band, meeting the assumption of the Zener equation that carriers tunnel into weakly bound states.

ACKNOWLEDGMENTS

We thank Stefan Glutsch, Andrey Kolovsky, Dirk Meinhold, and Vadim Lyssenko for helpful discussions. We acknowledge the financial support by Deutsche Forschungsgemeinschaft (Grants Nos. Ko 686/6, Le 747/11 and the Leibniz Preis).

*Electronic address: leo@iapp.de
†Electronic address: korsch@physik.uni-kl.de

[1] L. Esaki and R. Tsu, IBM J. Res. Dev. **14**, 61 (1970).
[2] E.E. Mendez, F. Agulló-Rueda, and J.M. Hong, Phys. Rev. Lett. **60**, 2426 (1988).
[3] G.H. Wannier, Phys. Rev. **117**, 432 (1960).
[4] J.E. Avron, J. Zak, A. Grossmann, and L. Gunther, J. Math. Phys. **18**, 918 (1977).
[5] G. Bastard, J. Bleuse, R. Ferreira, and P. Voisin, Superlattices Microstruct. **6**, 77 (1989).
[6] H. Schneider, H.T. Grahn, K.v. Klitzing, and K. Ploog, Phys. Rev. Lett. **65**, 2720 (1990).
[7] M. Nakayama, I. Tanaka, H. Nishimura, K. Kawashima, and F. Fujiwara, Phys. Rev. B **44**, 5935 (1991).
[8] K. Murayama, H. Nagasawa, S. Ozaki, M. Morifuji, C. Hamaguchi, A.D. Carlo, P. Vogel, G. Böhm, and G. Weimann, Superlattices Microstruct. **20**, 493 (1996).
[9] A. Sibille, J.F. Palmier, and F. Laruelle, Phys. Rev. Lett. **80**, 4506 (1998).
[10] M. Helm, W. Hilber, G. Strasser, R.D. Meester, F.M. Peeters, and A. Wacker, Phys. Rev. Lett. **82**, 3120 (1999).
[11] A.D. Carlo, P. Vogl, and W. Pötz, Phys. Rev. B **50**, 8358 (1994).
[12] X.-G. Zhao, Phys. Rev. B **62**, 5010 (2000).
[13] M. Holthaus, J. Opt. B: Quantum Semiclassical Opt. **2**, 589 (2000).
[14] G. Bastard, R. Ferreira, S. Chelles, and P. Voisin, Phys. Rev. B **50**, 4445 (1994).
[15] J. Krieger and G. Iafrate, Phys. Rev. B **33**, 5494 (1986).
[16] A. Sibille, Solid-State Electron. **32**, 1455 (1989).
[17] B. Rosam, D. Meinhold, F. Löser, V.G. Lyssenko, S. Glutsch, F. Bechstedt, F. Rossi, K. Köhler, and K. Leo, Phys. Rev. Lett. **86**, 1307 (2001).
[18] S. Glutsch and F. Bechstedt, Phys. Rev. B **60**, 16 584 (1999).
[19] C. Zener and H.H. Wills, Proc. R. Soc. London, Ser. A **145**, 523 (1934).
[20] C.F. Bharucha, K.W. Madison, P.R. Morrow, S.R. Wilkinson, B. Sundaram, and M.G. Raizen, Phys. Rev. A **55**, R857 (1997).
[21] M. Glück, A.R. Kolovsky, and H.J. Korsch, Phys. Rev. Lett. **83**, 891 (1999).
[22] M. Glück, A.R. Kolovsky, H.J. Korsch, and F. Zimmer, Phys. Rev. B **65**, 115302 (2000).
[23] M. Glück, A.R. Kolovsky, H.J. Korsch, and N. Moiseyev, Eur. Phys. J. D **4**, 239 (1998).
[24] M. Glück, A.R. Kolovsky, and H.J. Korsch, J. Opt. Soc. Am. B **2**, 694 (2000).
[25] M. Glück, M. Hankel, A.R. Kolovsky, and H.J. Korsch, J. Opt. B: Quantum Semiclassical Opt. **2**, 612 (2000).
[26] F. Keck, H.J. Korsch, and S. Mossmann, J. Phys. A **36**, 2125 (2003).
[27] C.P. Holfeld, F. Löser, M. Sudzius, K. Leo, D.M. Whittaker, and K. Köhler, Phys. Rev. Lett. **81**, 874 (1998).
[28] M.M. Dignam and J.E. Sipe, Phys. Rev. Lett. **64**, 1797 (1990).
[29] M.M. Dignam and J.E. Sipe, Phys. Rev. B **43**, 4097 (1991).
[30] N. Linder, Phys. Rev. B **55**, 13 664 (1997).
[31] S. Glutsch, F. Bechstedt, B. Rosam, and K. Leo, Phys. Rev. B **63**, 085307 (2001).
[32] M. Glück, A.R. Kolovsky, and H.J. Korsch, Phys. Rep. **366**, 103 (2002).
[33] M. Glück, A. Kolovsky, and H.J. Korsch, J. Phys. A **32**, 49 (1999).
[34] E.F. Schubert, E.O. Göbel, Y. Horikoshi, K. Ploog, and H.J. Queisser, Phys. Rev. B **30**, 813 (1984).
[35] R. Klann, H.T. Grahn, and K. Fujiwara, Phys. Rev. B **51**, 10 232 (1995).
[36] A. Ourmazd, W. Tsang, J. Rentschler, and D. Taylor, Appl. Phys. Lett. **50**, 1417 (1987).
[37] M. Wagner and H. Mizuta, Phys. Rev. B **48**, 14 393 (1993).
[38] In the first-order perturbation theory, the size of the gaps are defined by the values of the Fourier coefficient of the periodic potential. J.M. Ziman, *Principles of the Theory of Solids*, 2nd ed. (Cambridge University Press, Cambridge, 1972).